



HAL
open science

Energy cascade and the four-fifths law in superfluid turbulence

Julien Salort, Benoît Chabaud, Emmanuel Lévêque, Philippe-Emmanuel Roche

► **To cite this version:**

Julien Salort, Benoît Chabaud, Emmanuel Lévêque, Philippe-Emmanuel Roche. Energy cascade and the four-fifths law in superfluid turbulence. 2011. hal-00635578v1

HAL Id: hal-00635578

<https://hal.science/hal-00635578v1>

Preprint submitted on 25 Oct 2011 (v1), last revised 18 Jan 2012 (v2)

HAL is a multi-disciplinary open access archive for the deposit and dissemination of scientific research documents, whether they are published or not. The documents may come from teaching and research institutions in France or abroad, or from public or private research centers.

L'archive ouverte pluridisciplinaire **HAL**, est destinée au dépôt et à la diffusion de documents scientifiques de niveau recherche, publiés ou non, émanant des établissements d'enseignement et de recherche français ou étrangers, des laboratoires publics ou privés.

Energy cascade and the four-fifths law in superfluid turbulence

J. SALORT¹, B. CHABAUD¹, E. LÉVÊQUE² and P.-E. ROCHE¹

¹ *Institut Néel, CNRS/UJF - BP 166, F-38042 Grenoble cedex 9, France, EU*

² *Laboratoire de Physique de l'ENS Lyon, CNRS/Université Lyon 1, F-69364 Lyon cedex, France, EU*

PACS 47.37.+q – Hydrodynamic aspects of superfluidity; quantum fluids

PACS 67.57.De – Superflow and hydrodynamics

Abstract – The 4/5-law of turbulence, which characterizes the energy cascade from large to small eddies at high Reynolds numbers in classical fluids, is verified experimentally in a superfluid ⁴He wind tunnel, operated down to 1.56 K and up to $R_\lambda \approx 1100$. The result is corroborated by high resolution simulations of Landau-Tisza two-fluid model down to 1.15 K, corresponding to a residual normal fluid concentration below 3%, but with a lower Reynolds number of order $R_\lambda \approx 100$. Although the Kármán-Howarth equation (including a viscous term) is not valid *a priori* in a superfluid, we find that it provides an empirical description of the deviation from the ideal 4/5-law and allows us to identify an effective viscosity for the superfluid, whose value matches the normal fluid kinematic viscosity regardless of its concentration.

Introduction. – At low temperature but above $T_\lambda \approx 2.17$ K (at saturated vapor pressure), liquid ⁴He is a classical fluid, known as He I. Like air or water, its hydrodynamics behavior is described by the Navier-Stokes equation. When such a fluid is strongly stirred, its response becomes dominated by the non-linear term of the Navier-Stokes equation. The dynamics of such a system, known as “turbulence”, was first pictured by Richardson in 1920 and theorized by Kolmogorov in 1941 [1]. The energy, injected at a large scale, cascades down across the so-called “inertial” scales until it reaches dissipative scales. It can be shown from the Navier-Stokes equation that the energy flux across the scales results in skewed distribution for the velocity increments. This prediction, the only exact result known for turbulence, is sometimes referred to as the Kolmogorov 4/5-law. It is recalled later in this paper.

When liquid ⁴He is cooled below T_λ , it undergoes a phase transition. The new phase, called He II, can be described with the so-called two-fluid model [2]: an intimate mixture of a viscous “normal” component whose dynamics is described by the Navier-Stokes equation and an inviscid “superfluid” component with quantized vorticity. Both components are coupled by a mutual friction term. The fraction of superfluid component ρ_s/ρ_n — where ρ_s and ρ_n are respectively the densities of superfluid and normal components — varies with temperature, from 0 at T_λ to $+\infty$ in the zero-temperature limit. When He II is strongly stirred, a tangle of quantum vortices is generated. This kind of turbulent flow is often referred to

as “quantum turbulence” or “superfluid turbulence”. For an introduction to quantum turbulence, one may refer to [3, 4].

The focus of this letter is intense turbulence of He II at finite temperature ($T_\lambda > T \geq 1$ K). In such conditions, most of the superfluid kinetic energy distributes itself between the mechanical forcing scale (e.g. at 1 cm in [5]) and the typical inter-vortex scale (eg. at 4 μ m in [5]). Excitations at smaller scales are strongly damped by the viscosity of the normal component [3]. At scales larger than the inter-vortex spacing the details of individual vortices can be ignored (“continuous” or “coarse-grained” description) and superfluid turbulence can be investigated with the same statistical tools as classical turbulence. An important open question is how superfluid turbulence compares with classical turbulence. Experimental studies have revealed differences regarding the vorticity spectra [5, 6] but also striking similarities of decay rate scaling [7–10], drag force [11–13] and distribution of kinetic energy among scales with -5/3 power-law scaling [14, 15]. This scaling is consistent with the existence of a Kolmogorov energy cascade, however no direct proof has been reported yet, as stressed recently during the Quantum Turbulence Workshop in Abu Dhabi [16] (see also the conclusion of [17]).

The main goal of this paper is to test in a superfluid the 4/5-law which characterizes the energy cascade. To account for the departure from the ideal 4/5-law at small scale, the classical Kármán-Howarth equation is assessed. As a side result, we show that the superfluid inherits vis-

cosity from the normal component even when the normal fraction is very low, making it hardly distinguishable from a classical fluid using the signal of an inertial anemometer like a Pitot tube. To do this, we present experimental velocity fluctuations measurements obtained in a 1 m-long cryogenic helium wind tunnel at high Reynolds number as well as results from direct numerical simulations of the continuous two-fluid model at lower Reynolds number but fully resolved down to the inter-vortex scale.

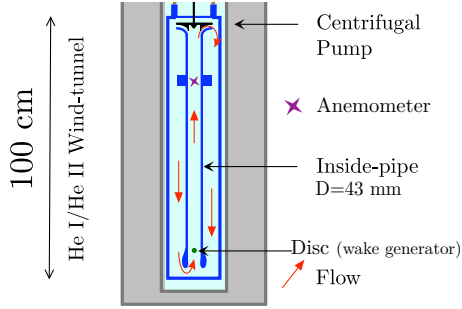


Fig. 1: Wind tunnel (in blue) in the cryostat (in gray)

Local velocity measurements. – Local velocity measurements have been realized in the wake of a disc in the wind tunnel sketched in figure 1. The disc diameter \varnothing_d is half the pipe diameter. The probe, located downstream at $x/\varnothing_d \approx 21$, was operated both above and below the superfluid transition, down to 1.56 K where $\rho_s/\rho_n \approx 5.8$. The wind tunnel is pressurized by more than 1 m of static liquid to prevent cavitation which could otherwise have occurred in He I. The turbulence intensity τ , defined as

$$\tau = \frac{\sqrt{\langle (v(t) - \langle v \rangle)^2 \rangle}}{\langle v \rangle} \quad (1)$$

where $v(t)$ is the local flow velocity and $\langle \cdot \rangle$ stands for time average, is close to 4.8 %, the mean velocity is $\langle v \rangle = 1$ m/s. The forcing length scale L_0 is defined from the frequency of the vortex shedding $f_0 = \langle v \rangle / L_0$, which is apparent on the velocity spectrum (see later). The typical Strouhal number, defined as

$$St = \frac{f_0 \varnothing_d}{\langle v \rangle} = \frac{\varnothing_d}{L_0} \quad (2)$$

is close to 0.35 both above and below the superfluid transition. At $T = 2.2$ K, where liquid helium is a classical fluid with kinematic viscosity $\nu = 1.78 \times 10^{-8}$ m²/s [18], the Reynolds number based on L_0 and the root-mean-square velocity is $Re = 1.8 \times 10^5$. The Taylor-microscale Reynolds number, R_λ , estimated as,

$$R_\lambda = \sqrt{\frac{20}{3}} Re \quad (3)$$

is found around $R_\lambda \sim 1100$.

The local anemometer is the probe labeled as ① in [15]. It is based on a stagnation pressure measurement (miniature ‘‘Pitot tube’’ probe). It measures the pressure overhead resulting from the stagnation point at the tip of the

probe, which is pointing upflow. Above the superfluid transition, the measured pressure $p_{\text{meas}}(t)$ can be written:

$$p_{\text{meas}}(t) = p(t) + \frac{1}{2} \rho v^2 \quad (4)$$

Following [14], a similar expression can be found for the measured pressure below the lambda transition using the continuous two-fluid description of He II

$$p_{\text{meas}}(t) = p(t) + \frac{1}{2} \rho_n v_n^2 + \frac{1}{2} \rho_s v_s^2 \quad (5)$$

where v_n is the velocity of the normal component and v_s the velocity of the superfluid component. Yet, physically, the probe is sensitive to the flux of momentum on its tip. It is therefore convenient [19] to rewrite the measured pressure in terms of the momentum velocity \vec{v}_m , based on the total mass flux and defined as

$$\rho \vec{v}_m = \rho_n \vec{v}_n + \rho_s \vec{v}_s \quad (6)$$

where $\rho = \rho_n + \rho_s$. This leads to

$$p_{\text{meas}}(t) = p(t) + \frac{1}{2} \rho v_m^2 + \frac{\rho_n \rho_s}{2\rho} (v_n - v_s)^2 \quad (7)$$

This equation is similar to the one standing in classical fluid (Eq. 4) plus an additional term. It has been argued theoretically [3] and shown numerically [20] that, in highly turbulent flows, the normal and superfluid components are nearly locked at inertial scales. Therefore, $(v_n - v_s)^2 \ll v_m^2$ and since $\rho_n \rho_s \leq \rho^2$, the last term in Eq. 7 can be neglected¹.

The calibrations of the probe above and below the superfluid transition are consistent with each other within 10 %. The difference comes from experimental uncertainties. In practice, the calibration obtained below T_λ , where the signal is cleaner, was used to determine the mean values obtained in normal fluid.

A numerical 4th-order Butterworth low-pass filter is applied to the velocity time series to suppress the probe organ-pipe resonance [15]. The filtered velocity time series are converted into spatial signals using instantaneous Taylor frozen turbulence hypothesis [21], ie. we relate the velocity at time t to the velocity at location x by:

$$v(t) = v(x) \text{ where } x = \int_0^t v(\tau) d\tau \quad (8)$$

The velocity power spectra and the velocity probability distribution are computed from the obtained space velocity series $v(x)$ and are shown in figure 2.

As expected, the power spectra are compatible with a Kolmogorov $k^{-5/3}$ scaling and the velocity distribution is nearly Gaussian. The spectra above and below the superfluid transition are nearly identical. The wave number are normalized by the forcing scale L_0 defined above. The observed cut-off at high k results from the finite resolution of the probes and not from a dissipative effect.

¹If the turbulence intensity is small, it is possible to get the same result with the weaker hypothesis: $\langle v_s \rangle = \langle v_n \rangle$, ie. normal and superfluid components are locked at large scale [19]. The slip velocity fluctuating term is of order τ^2 at most and thus can be neglected.

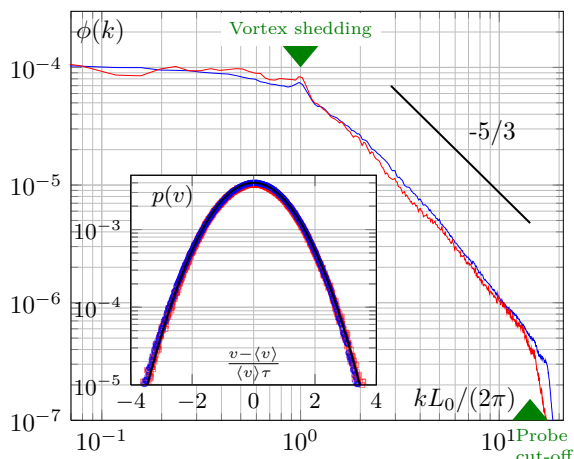


Fig. 2: Experimental 1D velocity power spectrum above and below the superfluid transition. Red line: $T = 2.2 \text{ K} > T_\lambda$ at $R_\lambda \approx 1100$. Blue line: $T = 1.56 \text{ K} < T_\lambda$. Inset: Velocity probability distribution above and below the superfluid transition. Black line: Gaussian distribution.

The longitudinal velocity increments, here along the streamwise direction, are defined as,

$$\delta v(x; r) = v(x + r) - v(x) \quad (9)$$

The distribution of $\delta v(x; r)$ for a given r , shown in figure 3, is fairly Gaussian at large scale ($r = L_0$) and clearly skewed on the negative side at smaller scales ($r = L_0/10$). The skewness $S(r)$ of this distribution is defined as,

$$S(r) = \frac{\langle \delta v(r)^3 \rangle}{\langle \delta v(r)^2 \rangle^{3/2}} \quad (10)$$

where $\langle \cdot \rangle$ stands for the space average. $S(r)$ is shown in the inset of figure 4.

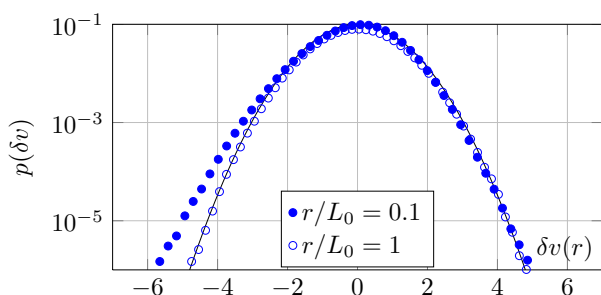


Fig. 3: Experimental histogram of the longitudinal velocity increments at large and intermediate scales in a superfluid turbulent flow ($T = 1.56 \text{ K}$). Solid black line: Gaussian distribution.

Above the superfluid transition, $S(r)$ is known to be directly linked to the energy rate of the Richardson cascade [22]. Its numerical value at the smallest resolved scale is fairly compatible with the typical classical value of -0.23 (a review of experimental values for R_λ between 208 and 2500 is given in [23]). The negative sign is a direct evidence that the energy cascades from large to small scales.

Below the superfluid transition, the value of the skewness is nearly identical to the one above the superfluid transition. This is a strong hint that energy cascades in a similar fashion above and below the superfluid transition.

More quantitatively, in classical homogeneous and isotropic turbulence, the third-order structure function is proportional at first order to the turbulent energy flux across the scales, ϵ . The 4/5-law states:

$$\langle \delta v(r)^3 \rangle \simeq -\frac{4}{5} \epsilon r \quad (11)$$

This equation, valid in the inertial range of the turbulent cascade, is often cited as the only exact result in classical fully developed turbulence (for asymptotically large Re). It is interesting to test its validity in quantum turbulence. In the experimental conditions of this work ($R_\lambda = 1100$), finite Reynolds number corrections to Eq. 11 are small [24].

To compare superfluid experimental data to this classical prediction, the mean experimental energy rate ϵ has to be estimated. It is not trivial to get an accurate estimate for ϵ from experimental data. A classical way is to use the third-order structure function and the 4/5-law, which gives reasonable estimates for $R_\lambda \gtrsim 1000$ [25, 26]. Since our aim is to assess the 4/5-law, we can not use this technique directly.

However, previous experiments found that ϵ does not change when the superfluid transition is crossed [15] and in our experiment, data are available with the same mean velocity above and below the superfluid transition. Therefore, we estimate ϵ from the 4/5-law using the He I recording — where it is known to hold since He I is a classical fluid — and we use that estimate to compensate the third-order velocity structure function obtained in He II. We find $\epsilon = (5.4 \pm 0.3) \times 10^{-3} \text{ m}^2/\text{s}^3$.

We obtain a “plateau” for nearly half a decade of scales, corresponding to the resolved inertial range of the turbulent cascade (see figure 4). The level of the “plateau” is comparable above and below the superfluid transition, within experimental uncertainty of around 25%. This is an experimental evidence that the 4/5-law (Eq. 11) remains valid in superfluid turbulence, at least for the largest inertial scales. Together with the invariance of the skewness, this is the first important result of this study.

Direct numerical simulations. — In this section, we processed velocity fields obtained in a stationary numerical simulation of He II with periodic boundary conditions. The numerical procedure is described in [20]. The simulated velocity fields have a resolution of 512^3 or 1024^3 . The simulated equations are summarized below,

$$\frac{D\vec{v}_n}{Dt} = -\frac{1}{\rho_n} \nabla p_n + \frac{\rho_s}{\rho} \vec{F}_{ns} + \frac{\mu}{\rho_n} \nabla^2 \vec{v}_n + \vec{f}_n^{ext} \quad (12)$$

$$\frac{D\vec{v}_s}{Dt} = -\frac{1}{\rho_s} \nabla p_s - \frac{\rho_n}{\rho} \vec{F}_{ns} + \vec{f}_s^{ext} \quad (13)$$

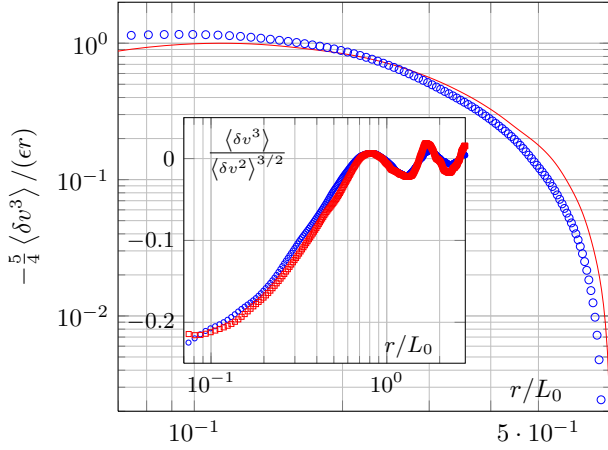


Fig. 4: Experimental third-order velocity structure function compensated by 4/5-law (Eq. 11) obtained in superfluid helium turbulent flow at $T = 1.56$ K (blue circles) and in classical liquid helium at $T = 2.2$ K (red squares). Inset: Skewness of the distribution of longitudinal velocity increments (same color code). The smallest abscissa $r/L_0 = 7 \times 10^{-2}$ corresponds to the probe cut-off. The oscillation at large scale corresponds to the frequency of the vortex shedding.

where indices n and s refer to the normal component and the superfluid one, respectively, \vec{f}_n^{ext} and \vec{f}_s^{ext} are external forcing terms, μ is the dynamic viscosity. The mutual coupling term is approximated by its first order expression:

$$\vec{F}_{ns} = -\frac{B}{2} |\vec{\omega}_s| (\vec{v}_n - \vec{v}_s) \quad (14)$$

where $\vec{\omega}_s = \nabla \times \vec{v}_s$ is the superfluid vorticity and $B = 2$ is taken as the mutual friction coefficient [27].

We impose that the simulation cut-off scale corresponds to the quantum inter-vortex scale δ , estimated from the quantum of circulation κ around a single superfluid vortex and from the average vorticity,

$$\delta^2 = \frac{\kappa}{\sqrt{\langle |\vec{\omega}_s|^2 \rangle}} \quad (15)$$

This truncation procedure was validated by the accurate prediction of the vortex line density in experiments [20].

The velocity power spectra for normal and superfluid components are shown in figure 5 in the very low and high temperature limits (resp. 1.15 K and 2.1565 K corresponding to $\rho_s/\rho_n = 40$ and $\rho_s/\rho_n = 0.1$). To allow closer comparison with the experiments, the Reynolds number Re is estimated as,

$$Re = \frac{L_0 \sqrt{\langle v_m^2 \rangle}}{\mu/\rho} \quad (16)$$

where $v_m = \frac{1}{\rho} (\rho_n v_n + \rho_s v_s)$ is the momentum velocity², $L_0 = \pi$ is the length corresponding to the forcing wave-number k_0 and the kinematic viscosity is μ/ρ . The power

²We used the one-dimensional rms, $v_{\text{rms,1d}} = \frac{v_{\text{rms,3d}}}{\sqrt{3}}$ to be comparable with experiments.

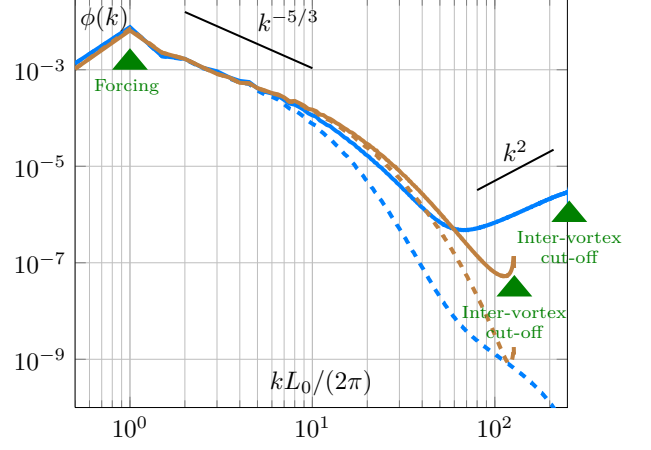


Fig. 5: Simulated 3D velocity power spectra. Solid lines are obtained from the velocity field of the superfluid component \vec{v}_s . Dashed lines are obtained from the velocity field of the normal component \vec{v}_n . The sky blue spectra were obtained at very low temperature ($T = 1.15$ K, 1024^3); the chocolate spectra were obtained at high temperature ($T = 2.1565$ K, 512^3). The smallest resolved scale matches the inter-vortex spacing. L_0 is defined as the forcing scale.

spectrum of the momentum velocity is not plotted but nearly matches the normal component spectrum at high temperature and the superfluid component spectrum at very low temperature, as expected.

The 1024^3 very low temperature simulation, where $\rho_s/\rho_n = 40$, and the 512^3 high temperature simulation, where $\rho_s/\rho_n = 0.1$, have nearly the same Reynolds number ($Re = 1960$ and $Re = 2280$ respectively), much smaller than the Reynolds number in the experiments (of order 1.8×10^5). Yet, in both cases, the spectra collapse at large scales close to a Kolmogorov-like $k^{-5/3}$ scaling but differ at smaller scales, named “meso-scales” [20]. In this range of meso-scales, larger than the inter-vortex scale but smaller than inertial scales, the superfluid component is no longer locked to the normal component. At the lowest temperatures, its energy distribution approaches a k^2 scaling, as evidenced in figure 5, which is compatible with the equipartition of superfluid energy.

The momentum velocity third-order longitudinal structure functions are computed by averaging the longitudinal increment along each three directions in one “snapshot” of the flow³.

One does not expect the 4/5-law to hold at such moderate Reynolds number. Yet, at high temperature: (i) the compensated third-order structure function reaches a maximum lower than one, as expected in classical turbulence at such Reynolds number [26], for which there is no clear separation between dissipative and inertial dynamics and (ii) the small-scale behavior goes typically like r^2

³We obtain similar results if the velocity increments are computed with the velocity field from the dominant component rather than v_m . The momentum velocity is convenient because it is defined for all temperatures and comparable to what is measured in experiments.

corresponding to the linear limit $\delta v(r) \sim r$. At very low temperature, the velocity field is no longer smooth at very small scale. It exhibits irregular fluctuations down to the smallest scales due to the equipartition noise. This results in a different behavior of $\langle \delta v(r)^3 \rangle$ at small scales, as shown in figure 6. As a side remark, reasons for large scale deviations are discussed in the classical turbulence literature [24].

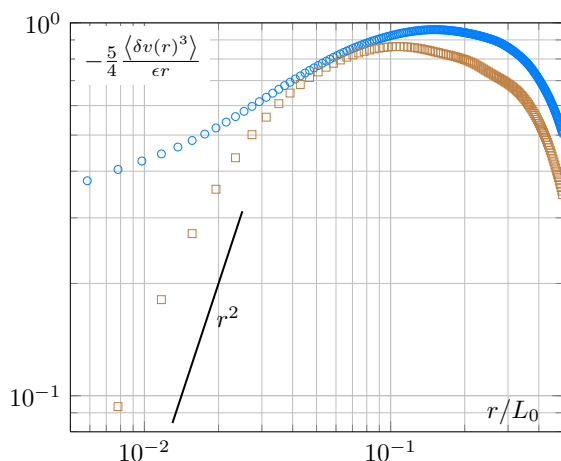


Fig. 6: Compensated third-order structure function obtained in numerical simulations at high temperature (chocolate squares) and very low temperature (sky blue circles) for nearly the same Reynolds numbers.

In the end of this paper, we address the departure from the ideal 4/5-law at small scale. In classical turbulence, this deviation, fully due to viscosity, can be derived from the Kármán-Howarth equation and generalizes the 4/5-law at small scales:

$$\langle \delta v(r)^3 \rangle + \frac{4}{5} \epsilon r = 6\nu \frac{d\langle \delta v(r)^2 \rangle}{dr} \quad (17)$$

This Kármán-Howarth equation is the expression of a scale-by-scale energy budget. Physically, the right-hand side of Eq. 17 corresponds to the energy that leaks out of the cascade due to viscous dissipation. The generalization of Kármán-Howarth to the two-fluid model contains a term associated with the coupling between the superfluid and normal components. It is delicate to integrate it into a form similar to Eq. 17. In the following, we follow an empirical approach and assess how the classical relation (Eq. 17) could be applied to the case of He II. Analogously to the classical case, an effective kinematic viscosity ν_{visc} can be defined in He II from the deviation to the 4/5-law in the small-scale side of the inertial range. Let's define $\mathcal{N}(r)$ as

$$\mathcal{N}(r) = \frac{\langle \delta v^3 \rangle + \frac{4}{5} \epsilon r}{6 \frac{d\langle \delta v^2 \rangle}{dr}} \quad (18)$$

The value of ϵ is a parameter of the simulation. In a Navier-Stokes fluid, the Eq. 17 implies that $\mathcal{N}(r)$ matches

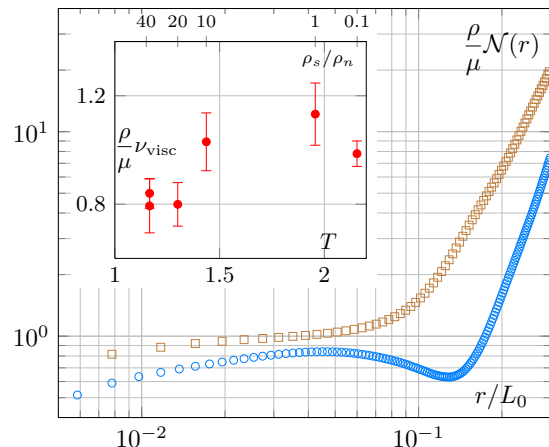


Fig. 7: Compensated effective viscosity versus scale obtained in numerical simulations at high temperature (chocolate squares) and very low temperature (sky blue circles) for nearly the same Reynolds number. Inset: effective viscosity estimated from the “plateau” of $\mathcal{N}(r)$ for various temperatures.

the kinetic viscosity μ/ρ from the “center” of the inertial range down to the smallest scales.

The values of $\mathcal{N}(r)$ computed from the simulated v_m fields³ in He II are plotted versus scale in figure 7 normalized by μ/ρ . For all simulated temperatures, ranging from 1.15 K ($\rho_s/\rho_n = 40$) where the superfluid component dominates to $\simeq 2.1565$ K ($\rho_s/\rho_n = 0.1$) where the normal component dominates, this plot shows a “plateau” in the inertial range, quite analogous to the Navier-Stokes case. It implies that the deviation to the 4/5-law can be described to some extent using an effective viscosity, down to very low temperature, even though the density of the normal component can be negligible. This shows that the mutual friction term in the superfluid equation (Eq. 13), although it is proportional to ρ_n/ρ cannot be neglected even at very low temperature and that it mimics to some extent a viscous term along the cascade. Nevertheless, $\mathcal{N}(r)$ deviates from the plateau at the smallest scales, where both components are no longer locked, especially at very low temperature (sky blue circles). This contrasts with classical turbulence where the “plateau” would extend down to the smallest scales [25].

From the value of this “plateau”, we define the effective viscosity ν_{visc} . The values obtained for ν_{visc} for various temperature and Reynolds conditions are shown in the inset of figure 7 compensated by μ/ρ . It is remarkable that this effective viscosity matches the dynamic viscosity of the normal component normalized by the total density within 20% at all temperatures. Thus, these simulations show that superfluid helium (He II) behaves as a viscous fluid in the inertial range of the turbulent cascade, when both components are nearly locked, even down to the lowest temperatures where the normal component fraction is smaller than 3%.

Concluding remarks. – Using longitudinal third-order structure functions, we have shown both experimentally and numerically that superfluid helium can undergo an energy cascade in the sense of Kolmogorov in stationary turbulence. In particular, our experimental data is quantitatively compatible with the classical 4/5-law in the inertial range. It is worth pointing out that the structure functions were analyzed in the usual way because the vortex singularities have been smoothed out, either by finite probe size effects or by the continuous simulation model. Without this low-pass filtering of the details of superfluid tangle, comparison with classical turbulence would be less straightforward.

The energy “leak” from the cascade was assessed applying the Kármán-Howarth equation on the velocity field of the simulation. We find that He II behaves as a viscous fluid in its inertial range, with an effective viscosity ν_{visc} inherited from the normal component, even down to the lowest temperature ($\rho_s/\rho_n = 40$). This conclusion does not extend down to the smallest (meso)-scales when both components are unlocked and quasi-equipartition evidenced. It is interesting to compare ν_{visc} to the effective viscosity ν_{eff} usually defined in the literature as [3],

$$\epsilon = \nu_{\text{eff}} \left(\frac{\kappa}{\delta^2} \right)^2 \simeq \nu_{\text{eff}} |\omega_s|^2. \quad (19)$$

This effective viscosity is compatible with ν_{visc} at high temperature [8], which can be understood writing that both components are roughly locked down to the (viscous) dissipation length scale:

$$\nu_{\text{eff}} = \epsilon |\omega_s|^{-2} \simeq \epsilon |\omega_n|^{-2} = \frac{\mu}{\rho_n} \simeq \frac{\mu}{\rho} = \nu_{\text{visc}} \quad (20)$$

However, ν_{eff} departs from the “viscous viscosity” ν_{visc} as the temperature is lowered [8–10], but becomes compatible with the “friction viscosity” $\nu_{\text{frict}} = \kappa \frac{\rho_n B}{2\rho}$. This latter viscosity can be derived from Eqs. 12 and 13 assuming that both components are unlocked at small scales which entails dissipation by friction of one fluid component on the other [28] (see [3] for a microscopic derivation). Thus, the definition of ν_{eff} encompasses the two dissipative mechanisms that occur in He II at finite temperature ($T > 1$ K): the “viscous dissipation”, ν_{visc} , that we discussed in this work and the “friction dissipation”, ν_{frict} . It would be interesting to understand how this empirical effective viscosity ν_{eff} (Eq. 19) depends on the relative weight of the two dissipation mechanisms and on a third dissipation mechanism relevant in the zero temperature limit: sound emission by vortex line [29–31]. The analytical integration of the Kármán-Howarth for the two-fluid model, which implies additional modeling, would open this perspective.

As a perspective, to further understand the mechanisms leading to viscous-like behavior, we point out a possible analogy with classical truncated Euler systems, in which the presence of an equipartitioned reservoir at small scales acts as a molecular viscosity at larger scales [32–34].

Acknowledgments. – This work benefited from the support of ANR (ANR-09-BLAN-0094) and from the computing facilities of PSMN at ENS Lyon and of GENCI-CINES (grant 2011-026380). We are grateful to Grégory Garde who designed and built the Helium wind tunnel and to Pierre Chanthib, Étienne Ghiringhelli, Pierre-Luc Delafin, Jacques Depont and Jean-Luc Kueny for their help. We thank Laurent Chevillard, Yves Gagne and Bernard Castaing and Roberto Benzi for interesting discussions.

REFERENCES

- [1] KOLMOGOROV A., *C. R. Acad. Sci. USSR*, (1941).
- [2] LANDAU L., *Phys. Rev.*, **60** (1941) 356.
- [3] VINEN W. F. and NIEMELA J. J., *J. Low Temp. Phys.*, **128** (2002) 167.
- [4] SERGEEV Y., *Nature Physics*, **7** (2011) 451.
- [5] ROCHE P.-E. *et al.*, *EPL*, **77** (2007) 66002.
- [6] BRADLEY D. *et al.*, *Phys. Rev. Lett.*, **101** (2008) 065302.
- [7] STALP S. R., SKRBK L. and DONNELLY R. J., *Phys. Rev. Lett.*, **82** (1999) 4831.
- [8] NIEMELA J., SREENIVASAN K. and DONNELLY R., *J. Low Temp. Phys.*, **138** (2005) 537.
- [9] CHAGOVETS T., GORDEEV A. and SKRBK L., *Phys. Rev. E*, **76** (2007) 027301.
- [10] WALMSLEY P. and GOLOV A., *Phys. Rev. Lett.*, **100** (2008) 245301.
- [11] ROUSSET B. *et al.*, in proc. of 15th Int. Cryo. Eng. Conf. Vol. 34 1994 pp. 317–320.
- [12] SMITH M. R., HILTON D. K. and SCIVER S. W. V., *Phys. fluids*, **11** (1999) 751.
- [13] FUZIER S. *et al.*, *Cryogenics*, **41** (2001) 453.
- [14] MAURER J. and TABELING P., *EPL*, **43** (1998) 29.
- [15] SALORT J. *et al.*, *Phys. fluids*, **22** (2010) 125102.
- [16] BENZI R., in *Classical and Quantum Turbulence Workshop, Abu Dhabi*, May 2nd, 2011.
- [17] SAMUELS D. C. and KIVOTIDES D., *Phys. Rev. Lett.*, **83** (1999) 5306.
- [18] DONNELLY R. and BARENGHI C., *J. Phys. Chem. Ref. Data*, **27** (1998) 1217.
- [19] KIVOTIDES D. *et al.*, *EPL*, **57** (2002) 845.
- [20] SALORT J. *et al.*, *EPL*, **94** (2011) 24001.
- [21] PINTON J.-F. and LABBÉ R., *J. Phys. II*, **4** (1994) 1461.
- [22] MONIN A. and YAGLOM A., *Statistical Fluid Mechanics* (MIT Press, Cambridge) 1971.
- [23] CHEVILLARD L. *et al.*, *Physica D*, **218** (2006) 77.
- [24] ANTONIA R. A. and BURATTINI P., *J. Fluid Mech.*, **550** (2006) 175.
- [25] MOISY F. *et al.*, *Phys. Rev. Lett.*, **82** (1999) 3994.
- [26] ISHIHARA T. *et al.*, *Annu. Rev. Fluid Mech.*, **41** (2009) 165.
- [27] BARENGHI C. and DONNELLY R., *J. Low Temp. Phys.*, **52** (1983) 189.
- [28] ROCHE P.-E. *et al.*, *EPL*, **87** (2009) 54006.
- [29] NORE C. *et al.*, *Phys. Rev. Lett.*, **78** (1997) 3896.
- [30] VINEN W., *Phys. Rev. B*, **61** (2000) 1410.
- [31] LEADBEATER M. *et al.*, *Phys. Rev. Lett.*, **86** (2001) 1410.
- [32] KRAICHNAN R. and CHEN S., *Physica D*, **37** (1989) 160.
- [33] CICHOWLAS C. *et al.*, *Phys. Rev. Lett.*, **95** (2005) 264502.
- [34] BOS W. and BERTOGLIO J.-P., *Phys. fluids*, **18** (2006) 071701.